ELSEVIER

Journal of Magnetism and Magnetic Materials 175 (1997) 160–176

journal of magnetism and magnetic materials

Soft X-ray photoemission electron microscopy as an element-specific probe of magnetic microstructures

C.M. Schneider*

Inst. f. Physik, Joh. Gutenberg-Universität, Staudingerweg 7, D-55099 Mainz, Germany

Abstract

Photoemission electron microscopy has matured into a versatile analytical technique on mesoscopic length scales. Applications range from surface physics or chemistry to biology. When operated with circularly polarized light in the soft X-ray regime, however, photoemission microscopy offers a unique access to many aspects in surface and thin film magnetism by combining magnetic and chemical information. Exploiting the high brilliance and circular polarization available at a helical undulator beamline, the lateral resolution in the imaging of magnetic domain structures may be pushed well into the sub-micrometer range. By means of a newly designed photoemission microscope not only domains, but also domain walls can be selectively investigated under these circumstances. The high sensitivity of the technique yields a sizable magnetic contrast even from ultrathin films in the monolayer regime. The combination of chemical selectivity and information depth can be employed to investigate the magnetic behavior of buried layers and covered surfaces. This approach offers a convenient access to magnetic coupling phenomena in magnetic sandwich structures.

PACS: 61.16.M; 75.60.C; 78.20.L

Keywords: Photoemission spectroscopy; Domain imaging; Magnetic circular dichroism

1. Introduction

The physics of magnetic microstructures has always been a research area with strong links to technological applications. With the progress in magnetic information storage and the development of high-density magnetic storage media these links are becoming even more important. The performance of a magnetic storage device, for example, a hard-disk drive, is crucially determined by the controlled creation of well-defined magnetic domains which carry the information ('bits'). A characterization of these magnetic microstructures as well as an understanding of the processes during magnetization reversal are therefore important issues. The demand for higher storage densities is met by reducing the average bit sizes. Currently, systems on the market employ bit sizes with lateral dimensions of several hundred nanometers.

* On leave of absence from Max-Planck-Institut f. Mikrostrukturphysik, Am Weinberg 2, D-06120 Halle (Saale). Tel.: 49 345 558250; fax: 49 345 5511223; e-mail: schneiderc@port.exp.bessy.de.

PII S0304-8853(97)00173-X

A reduction of the bit size, however, also diminishes the magnetic stray field above the bit which must be picked up by the reading head in order to retrieve the written information. This situation requires the sensitivity of the read-out procedure to be increased. A considerable improvement is achieved by exploiting new physical phenomena, such as giant magneto-resistance (GMR) in interlayer-coupled multilayers. Inductive or conventional magneto-resistive heads may therefore soon be replaced by GMR-based devices. This illustrates that the fundamental questions and aspects of thin film and surface magnetism are becoming more and more relevant for both storage materials and read/write heads.

A micromagnetic probe adapted to this particular situation should ideally combine high lateral resolution with surface sensitivity and chemical selectivity. The latter criterion arises from the chemical complexity of the storage materials which are currently relevant for technological applications. A thorough understanding of their magnetic properties must take into account the magnetic contribution of the individual chemical constituents. These requirements pose a considerable challenge to established domain-imaging techniques. In magneto-optical Kerr microscopy [1, 2], for instance, the lateral resolution is limited by the photon wavelength. Lorentz microscopy [3, 4] is based on the transmission of an electron beam and thus lacks surface sensitivity. This situation stimulated and still drives the development of various high-resolution approaches to magnetic imaging involving alternative physical principles of magnetic contrast formation. These are, for example, scanning electron microscopy with spin polarization analysis (SEMPA) [5–7], magnetic force microscopy (MFM) [8–10], scanning near-field optical microscopy (SNOM) [11], magnetic X-ray microscopy with zone plates (XRM) [12], or spin-polarized low-energy electron microscopy (SP-LEEM) [13]. For some of these techniques (SEMPA, SP-LEEM) spatial resolution capabilities of several 10 nm have already been demonstrated. Most of these techniques have in common, however, the lack of chemical specificity (in LEEM some information may be drawn from work function changes between areas of different chemical composition). This limitation can be overcome by exploiting the various forms of magnetic X-ray dichroism as a contrast mechanism. The desired surface sensitivity is then achieved by means of a photoemission electron microscope, whereas the bulk properties may be probed on the basis of the same magnetodichroic phenomena by X-ray microscopy (see the contribution by Schütz et al. in this issue).

In order to image magnetic domains with elemental specificity in a photoemission electron microscope, two different approaches have been pursued. First, the excitation (photon) energy is chosen such that it corresponds to a characteristic electronic level in the solid and the image is formed by low-energy secondary electrons [14]. This technique is most popular because the instrument does not require an energy filter with imaging capabilities. The light source, however, must be tunable in the X-ray regime which restricts the experiments to synchrotron radiation facilities. It is the method of choice with the so-called cathode or immersion lens photoemission microscopes. Since the literature often refers to this type of instruments by the acronym PEEM (PhotoEmission Electron Microscope), we adhere to this practice. Nevertheless, it should be noted that the instrument images secondary electrons rather than genuine photoelectrons, as soon as X-rays are used. In the second technique, the photon energy is chosen higher than the absorption edge so that the image can be acquired with direct photoelectrons from the characteristic levels [15]. In this case the photon energy can be fixed, but the image must be energy-filtered in order to select a certain photoemission line. This technique has first been employed in imaging electron spectrometers [16] which may be seen as another form of photoemission microscopes. Common to both approaches is that they offer a unique combination of magnetic sensitivity and chemical selectivity. The differences with respect to the experimental performance will be discussed in more detail in the following section.

2. Magnetic contrast mechanisms in photoemission microscopy

The magnitude and direction of the local magnetization $\boldsymbol{M}$ at a surface are directly reflected in the

spin polarization vector $\boldsymbol{P}$ of the low-energy secondary electrons emitted from this surface [17]. This proportionality is exploited in SEMPA to obtain a pixel-by-pixel map of the lateral magnetization distribution by scanning a primary electron beam across the surface. The magnitude and the spatial orientation of the secondary electron polarization $\boldsymbol{P}$ at each point of the scanning process is determined by means of a spin polarimeter.

For a direct imaging technique such as photoemission electron microscopy, however, an explicit analysis of the electron spin polarization would be extremely difficult to implement. The reason is the spin-dependent scattering of the electron beam that forms the working principle of basically all existing spin polarimeters [18, 19]. Among other problems, the scattering process involves a loss of intensity of the electron beam left for imaging by 2–3 orders of magnitude and will thus substantially impair the image quality. If the magnetic information cannot be drawn directly from the electron spin, one must have a physical mechanism which translates the magnetization distribution at the surface into a signal that can be measured in the *intensity* of the emitted electrons. It should be noted in this context that already in 1957 the imaging of magnetic domains by means of a photoemission electron microscope was reported [20]. These experiments exploited the deflection of the emitted electrons due to the Lorentz force in the magnetic stray field at the sample surface. This contrast may be seen as the emission counterpart to transmission Lorentz microscopy. The Lorentz force contrast mechanism requires reasonably high magnetic stray fields and, therefore, works best with hard magnetic materials [21]. It does not provide, however, any elemental selectivity.

In order to obtain elemental selectivity the contrast mechanism must be closely connected to the electronic states involved in the photoexcitation process. A number of pioneering experiments in X-ray absorption [22] and photoemission spectroscopy [23, 24] have recently established the phenomenon of *magnetic dichroism*. Magnetic dichroism (MD) means that the structure of a photoabsorption or -emission spectrum and the relative intensity of the spectral features vary distinctly with a change of the magnetization direction or a change

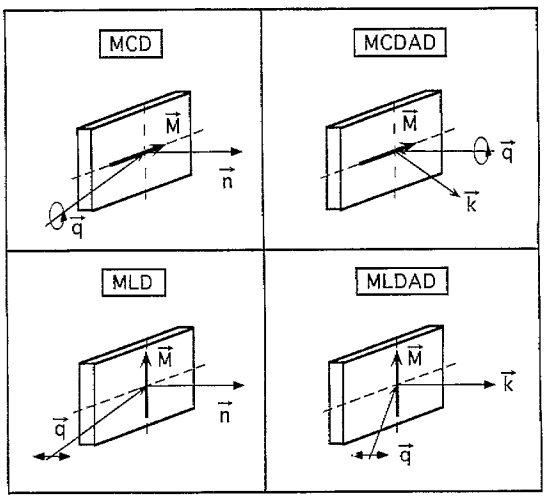

Fig. 1. Geometrical relationship of the photon wave vector q, magnetization M, electron wave vector k, and surface normal n associated with the various types of magnetic dichroism observed with circularly and linearly polarized light.

of the polarization state of the incident light. The microscopic origin of this effect involves the interplay of spin–orbit coupling and exchange interaction in the electronic states which participate in the photoexcitation. With respect to the application as a contrast mechanism in photoemission microscopy significant differences exist between magnetic dichroism in photoabsorption and photoemission. These differences result, for example, in specific experimental geometries which are needed to observe a particular type of magnetic dichroism (Fig. 1).

2.1. Magnetic dichroism in photoabsorption (MD)

Among the various kinds of magneto-dichroic phenomena magnetic dichroism with circularly polarized soft X-rays (MCD or MCXD) may be conceptually the easiest to understand. The circularly polarized light is used to excite electrons from a spin–orbit split core level, for example, a p level. Due to the spin–orbit coupling in the core electronic state the transition matrix element becomes spin-dependent causing the excited electrons to be spin-polarized. This effect is known as optical spin

orientation or Fano effect [25] and appears if spin–orbit coupling is present in the occupied or empty state, or in both. The spin quantization axis of the electrons is defined by the photon spin, i.e., the helicity of the circularly polarized light (or equivalently, the photon wave vector q). The spin polarization of electrons excited from the two spin–orbit split levels ($p_{1/2}$ and $p_{3/2}$) has opposite sign. In a photoabsorption process, the unoccupied state which the electron is excited into is located between the Fermi energy E_F and the vacuum level. The corresponding unoccupied density of states in a ferromagnet differs for spin-up and spin-down electrons, thereby constituting the magnetic moment. The density of states is made up predominantly from d-like valence electrons. The spin splitting in these states comes about by the exchange interaction and the fact that the electronic system can find a state of lower total energy if the spins are oriented parallel. As a consequence, there is an imbalance in the occupied states resulting in more occupied spin-up (majority) states than spin-down (minority) states. In turn, we have more empty minority than majority spin states. The spatial orientation of the *magnetic* spin quantization axis is given by the sample magnetization M (majority spin antiparallel, minority spin parallel to M).

We now consider a situation in which the two spin quantization axes defined by q and M are collinear. A spin-up electron excited from a 2p level then directly corresponds to a majority spin electron in the ferromagnet. Since the spin must be preserved during the optical excitation, the transition can only take place into an unoccupied majority spin state. Because the majority spin DOS available is small, the transition probability is small, too. On the contrary, the transition probability for a minority spin electron is higher, because the corresponding unoccupied DOS is larger. Measuring the absorption cross section will therefore show a marked difference for the excitation of the same level with light of opposite helicity. The effect exhibits the opposite sign for the other spin–orbit split level. It also changes sign upon magnetization reversal, because the spatial orientation of minority and majority electrons depends only on the direction of M (Fig. 2). Magnetic dichroism therefore effectively acts like an 'internal spin detector', in which the excited spin-polarized core electron is used to probe the magnetic state determined by the valence electrons. The phenomenon of MCD was first shown to exist in experiments at the Fe K-edges [22]. Using the $L_{2,3}$ absorption edges of the transition metals is more convenient, because the magnitude of the magneto-dichroic signal profits from both the large spin–orbit interaction in the core states and the large exchange coupling in the valence states [26]. This type of magnetic circular dichroism can be directly employed as a magnetic contrast mechanism in a X-ray microscope.

In order to serve as a magnetic contrast mechanism in photoemission microscopy the dichroism must be transferred to the emitted electrons. This takes place in two steps. The photoexcitation of a 2p electron creates a core hole in the 2p shell. This core hole decays within a certain lifetime either due to the emission of fluorescence radiation or due to an Auger process. In the latter case, the magnetic dichroism can be directly observed in the partial or Auger electron yield [15]. A use of the energetic Auger electrons for imaging purposes, however, requires the microscope to be equipped with an appropriate imaging energy filter. This contrast mechanism has already been successfully employed in an imaging electron spectrometer for studies of the magnetic interlayer coupling in the Fe/Cr/Fe system [27]. The photoexcitation of a characteristic absorption edge combined with the image formation by Auger electrons renders this approach extremely element selective and surface sensitive. The information depth is determined by the inelastic mean free path of the Auger electrons.

Due to its high kinetic energy the Auger electron suffers inelastic scattering events and generates a cascade of low-energy secondary electrons on its way through the solid. By this mechanism the magnetic dichroism in the Auger electron yield is converted into a difference in the flux of the secondary electrons (secondary electron yield). The magneto-dichroic signal carried by the low-energy secondary electron yield may be somewhat smaller than the corresponding dichroism in the Auger electrons. The reduction is due to secondary electrons which stem from direct photoemission events involving core levels with binding energies smaller than that

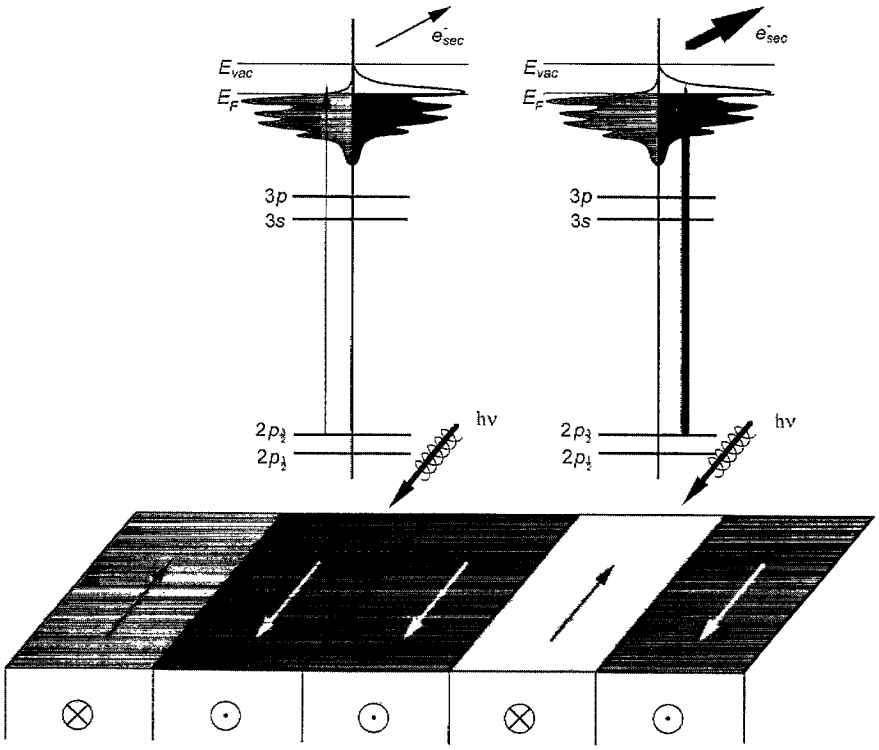

Fig. 2. Principle of MCD in photoabsorption.

of the absorption edge used, and which do not show the same dichroic response. Still, measurements of MCD in the so-called total yield mode exhibit a strong magneto-dichroic signal for the transition metal $L_{2,3}$ edges [26]. It should be kept in mind that the total yield is dominated by the behavior of the low-energy secondary electrons (kinetic energies up to about 10 eV) simply due to their large number. For the purpose of magnetic imaging this is a very fortunate case, because a strong MCD signal coincides with a large electron intensity. This situation perfectly fits the application of a cathode lens microscope without imaging energy filter (see Section 3). Such an instrument has a pronounced low-pass characteristics of its electron-optical transmission function [28]. The imaging process involves an effective integration over the electron distribution weighted by the transmission function. Since the low-energy secondary electrons have lost any specific information about characteristic electronic states in the solid, chemical selectivity in the imaging is only introduced via the photoexcitation step. MCD in the low-energy secondary yield is currently the most popular contrast mechanism employed in photoemission electron microscopy, and most of the results discussed in the remaining chapters have been obtained with this technique.

According to the orientational characteristics of MCD sketched in Fig. 1 the dichroism becomes largest for $\boldsymbol{M}$ and $\boldsymbol{q}$ being collinear. More precisely, the magneto-dichroic signal A, i.e., the magnetic contrast, varies as $A \sim \boldsymbol{q} \cdot \boldsymbol{M}$. One can therefore expect the following behavior of the magnetic contrast in a PEEM: magnetic domains with a local magnetization vector parallel or antiparallel to $\boldsymbol{q}$ will exhibit a dark/bright contrast, because areas with $\boldsymbol{M}$ parallel and antiparallel to $\boldsymbol{q}$ have different secondary electron yields. Magnetic domains with $\boldsymbol{q} \perp \boldsymbol{M}$, however, exhibit no magnetic contrast.

The same magnetic domain pattern will lead to a completely different image if linearly polarized light is used. In this case, the magnetic contrast arises due to magnetic linear dichroism in photoabsorption (MLD) which may be seen as the high-energy counterpart of the familiar transverse magneto-optical Kerr effect [29]. The dichroic signal becomes largest for a magnetization vector $\boldsymbol{M}$ oriented perpendicular to the plane defined by $\boldsymbol{q}$ and the electric field vector $\boldsymbol{E}$ of the incident linearly polarized light. In other words, assuming the same experimental geometry (Fig. 1), the magnetic linear dichroism selects those domains for which the magnetic contrast vanishes with circularly polarized light and vice versa.

2.2. Magnetic dichroism in photoemission (MDAD)

Once the photoexcitation of the core electron takes place into an empty state above the vacuum level, one may observe a magnetic dichroism in the direct ('true') photoelectrons. It is important to point out the differences to the situation discussed in Section 2.1. First, the influence of the exchange interaction on the electronic states far above the Fermi level is small. As a consequence, the exchange-splitting in the empty states into which the photoexcitation takes place practically vanishes. In order to generate a magnetic dichroism under these circumstances, both spin–orbit coupling and exchange interaction must be present in the occupied state. In a core level, the exchange-induced state splitting is small, thus, leading to relatively small magneto-dichroic signal of the order of several percent [23]. Second, the photoelectron undergoes not only multiple inelastic, but also elastic scattering processes before leaving the crystal. The influence of the latter on the photoelectron intensity is summarized under the label of photoelectron diffraction. Due to photoelectron diffraction of the core-level photoelectron also the electron wave vector $\boldsymbol{k}$ becomes an important parameter [30]. As a consequence, not only the photoelectron intensity but, in particular, the magnetic dichroism exhibits a complex angular variation [31, 32]. The magnitude of the magneto-dichroic signal depends in a complicated way on the relative orientation of $\boldsymbol{q}$, $\boldsymbol{M}$, $\boldsymbol{k}$ and $\boldsymbol{n}$, whereby $\boldsymbol{n}$ denotes the surface normal of the sample. A small selection of basic experimental geometries which result in a non-zero magneto-dichroic signal with circularly (MCDAD) and linearly polarized light (MLDAD) are given in the right-hand column in Fig. 1.

With respect to the application of MDAD as a contrast mechanism in photoemission microscopy, the issues of energetic and angular resolution have to be considered. Spectroscopic investigations of the 2p and 3p levels in the transition metals revealed that the dichroic signal often takes the form of a plus/minus feature, i.e., it changes sign over the photoemission line. The imaging instrument must therefore be capable of selecting electrons only within a narrow window of well-defined kinetic energy. An imaging energy filter is mandatory for this purpose and has also been implemented successfully into cathode lens microscopes [33]. This leaves the issue of angular resolution. Since in MDAD the magnetic dichroism may vary also strongly with the electron wave vector $\boldsymbol{k}$, integrating the emitted electrons over a large solid angle will result in a partial or total cancellation of the dichroic signal. In order to preserve a high magnetic contrast, the electron optics of the microscope should also provide a proper angular resolution. In an immersion lens microscope, however, just the opposite is the case. Due to the strongly accelerating electrostatic field between sample and cathode lens, electrons emitted into a relatively large solid angle can contribute to the image. This is the reason why the exploitation of MDAD in magnetic domain investigations has only been demonstrated in imaging electron spectrometers [16]. In these devices the region between sample and entrance of the electron optical column is intentionally kept field-free [34]. The drawback of an energy- and angle-resolved approach, of course, is a significantly reduced electron intensity available for the imaging process.

2.3. Separation of the magnetic information

In a single image the magnetic information due to any magnetic dichroism is superimposed onto the contrast generated by the sample topography or an inhomogenous distribution of the individual chemical constituents of the sample. For the case of

magnetic circular dichroism the magnetic contrast can be extracted in two ways. The first one exploits the property of MCD that by virtue of the helicity change the magnetic contrast is reversed, whereas other contrast mechanisms remain unaffected. Therefore, non-magnetic contributions are eliminated by subtracting two images acquired at opposite light helicities

$$I_M(x, y) = I_+(x, y) - I_-(x, y), \quad (1)$$

$$I_{NM}(x, y) = I_+(x, y) + I_-(x, y), \quad (2)$$

$$A(x, y) = I_M(x, y)/I_{NM}(x, y). \quad (3)$$

In the same way, the magnetic information can be eliminated by summing up the two images. The result is a complete separation of magnetic and non-magnetic contributions to the contrast. Normalizing $I_M(x, y)$ to $I_{NM}(x, y)$ puts the magnetic signal on an absolute scale and serves as a bright-field correction. The normalized quantity is called intensity asymmetry $A(x, y)$ or magneto-dichroic signal. The second procedure makes use of the spectral characteristics of MCD. In the case of the $L_{2,3}$ edge, for instance, the magnetic dichroism has opposite sign for the L_2 and the L_3 edge for a given helicity and magnetization. One may therefore apply operations (1)–(3) to two images acquired at the L_2 and L_3 edges. This procedure, however, yields only a partial decomposition of magnetic and non-magnetic contrast, because both the magnitude of the dichroism at the two edges and the ratio of peak intensity to background differ. It is thus less favorable and may lead to difficulties if small magnetic signals are concerned. A complete separation of magnetic and non-magnetic contributions can only be achieved when comparing two images recorded at the same edge for opposite light helicities.

3. Experimental details and technical issues

Most of the experimental results referred to in this contribution have been obtained by means of a newly designed cathode lens microscope using elliptically polarized synchrotron radiation in the soft X-ray regime. The experimental key features will be briefly described in the following.

3.1. Sources for elliptically polarized soft X-rays

The experiments used beamlines at the German storage ring BESSY (Berlin) and the European Synchrotron Radiation Facility (ESRF) in Grenoble. In both cases the beamline is optimized for the operation with elliptically polarized light. At BESSY the light is generated in a bending magnet section of the storage ring and dispersed by a plane grating monochromator (PM 3). The polarization state of the light is chosen by a movable premirror system [35]. When emitted within the storage ring plane the light is linearly polarized, with the electric field vector being parallel to the plane of the electron orbit. Above and below this plane the light is elliptically polarized with opposite helicities. By means of the premirror system either the in-plane radiation or a defined portion of the beam above or below the storage-ring plane can be selected. The degree of circularity depends on the off-plane angle (typically, 0.3–0.6 mrad). Between 700 and 900 eV photon energy it reaches values of the order of $P_C \approx 70\%$ [35]. The beamline covers a photon energy range up to about 1000 eV.

The beamline BL 26 at the ESRF operates with light from a particular insertion device, the so-called helical undulator [36]. In principle, an undulator consists of two linear magnetic structures which are facing each other at a defined distance ('gap'). Each structure is composed of a periodic arrangement of magnetic pole pieces with alternating orientations of the magnetic field vector. An electron bunch passing through the gap between the magnetic structures experiences a periodic deviation (undulation) which is superimposed on its original trajectory. The light pulses emitted along the undulator axis during subsequent deflections of the electron bunch have a certain phase relation and may interfere constructively for a certain range of wavelengths. Due to this interference the undulator generates a high-photon flux which is limited, however, to a narrow energy band. The energy band can be shifted by changing the undulator gap. In a helical undulator, the magnetic structures can also be shifted along the undulator axis relative to each other ('phase') resulting in a complicated electron trajectory. In this case the emitted light is elliptically polarized and the helicity for a given

wavelength is chosen by adjusting the gap and the magnetic phase of the undulator properly.

The beamline BL 26 is fed with the light from a twin helical undulator [36]. Each of the two modules may be set to generate circularly polarized light with the opposite helicity which is focused on the same spot of the sample by means of a spherical grating monochromator of the Dragon type [37]. The light helicity at the sample is therefore selected by blocking one of the two beams. The degree of circularity in the soft X-ray regime is reportedly better than 80% [38].

3.2. *The photoemission microscope*

The photoemission electron microscope used in our experiments employes a new design which differs in several respects from earlier set-ups (Fig. 3). The principle of image formation involves an electrostatic tetrode lens and a contrast aperture [39]. Instead of using a fixed aperture a set of circular diaphragms with different sizes were mounted onto a slide which can be positioned in situ by piezomotors. Thus, the contrast aperture can be conveniently adjusted during the operation of the instrument, and its size can be selected between 500 and 50 μm. The smaller the diameter of the aperture, the better is the lateral resolution that can be achieved. In order to reduce the influence of non-spherical aberrations in the electron optics an electrostatic octopole stigmator has been inserted into the back-focal plane of the objective. With the octopole arrangement astigmatism can be corrected in any rotational orientation. In addition, the stigmator may serve as an x, y-deflector by means of which the field of view can be changed without moving the sample. The size of the field of view can be selected by an iris aperture which is important for microspectroscopy applications. The image is magnified by a two stage projective, intensified by a multichannel plate, and converted into visible light by means of a scintillator crystal. It can be recorded by a conventional and a slow-scan CCD camera system.

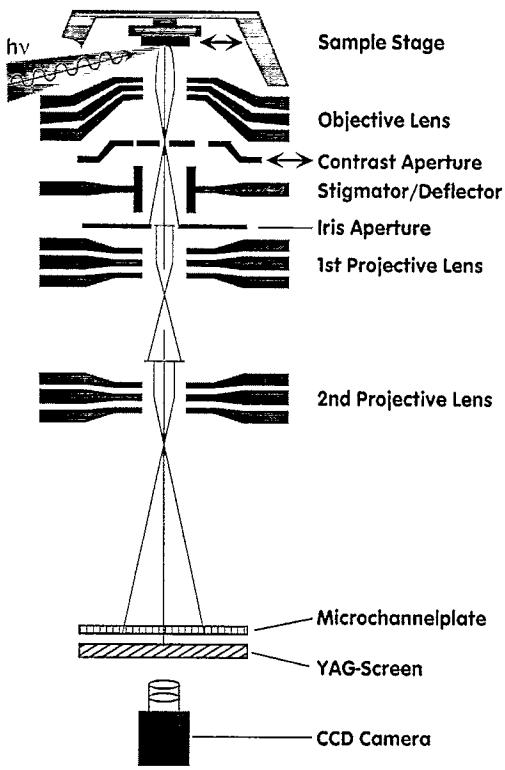

Fig. 3. Schematic set-up of the photoelectron emission microscope (Focus IS-PEEM) with integral sample stage and variable contrast aperture.

The sample holder forms an integral part of the electron optical column. This way uncontrolled motions of the sample relative to the objective lens are greatly reduced, and the image quality is much less affected by vibrations. In order to move the sample laterally in the object plane two orthogonal piezo-driven microslides are used. These allow a convenient positioning of the sample within a scan area of 5 mm × 5 mm. The sample itself is mounted onto a Mo carrier plate which can be transferred into and out of the microscope.

There is always a compromise between lateral resolution and field of view. The microscope can therefore be operated in two imaging modes: (i) a survey mode, and (ii) a high-resolution mode. The high-resolution mode employs high extraction voltages resulting in a field of view of about 20 μm. Topography measurements in threshold photoemission using a Hg high-pressure discharge source yielded a lateral resolution of better than 35 nm. The survey mode works with low-extraction fields and has inferior lateral resolution. The field of view may be as high as 700 μm.

When installed at the beamline, the electron-optical axis of the microscope is oriented parallel to the storage ring plane, with the angle of incidence of the light being fixed to 25°. With this geometry, different types of magnetic dichroism with linearly or circularly polarized light can be exploited at both bending magnet and undulator beamlines.

4. Artificial microstructures

In order to characterize the performance of the microscope with respect to chemical and magnetic imaging, we investigated several microstructured samples. The first one consisted of a 30 nm thick permalloy film ($Fe_{19}Ni_{81}$) on a Si wafer. The regular pattern of squares with a period of 25 μm was created by depositing the permalloy through a mesh. A single image of this structure taken at the Fe L_2 or L_3 edge reveals a surprising contrast (Fig. 4). The permalloy squares appear dark, whereas the uncovered Si surface shows up bright. This apparent contradiction is resolved, when studying the absorption (yield) spectra in selected areas. For this purpose the signal in the desired area of the image is integrated on-line and recorded as a function of photon energy. The resulting X-ray absorption spectra from the permalloy patches and the Si substrate (area of integration: 7 μm × 7 μm) show the characteristic Fe and Ni absorption lines and an almost featureless distribution, respectively. The electron yield from the Si substrate, however, is always higher on an absolute scale than the permalloy signal. This is the reason, why the permalloy patches appear darker. The data in Fig. 4 represent a nice example for the kind of chemical microanalysis that can be carried out with a PEEM. Considering the good signal-to-noise ratio of the spectra one may obtain local chemical information even from sub-μm-sized areas. The sensitivity is outlined by a close inspection of the spectra in Fig. 4, which reveal the presence of a small amount of Ni on the Si grid. This is due to some out-diffusion of Ni from the permalloy patches presumably caused by a thermal treatment of the sample.

The magnetic information becomes visible after subtracting images according to Eqs. (1) and (2). For technical reasons on this sample only a $L_3 - L_2$ difference image could be obtained. The image shown in Fig. 5 represents the magnetic domain structure seen at the Fe $L_{2,3}$ absorption edge. Most of the squares in the field of view reveal a very regular pattern, consisting of four triangular domains. The direction of light incidence is parallel to the horizontal side of the squares. From the contrast distribution in a square we can directly reconstruct the spatial distribution of the magnetization,

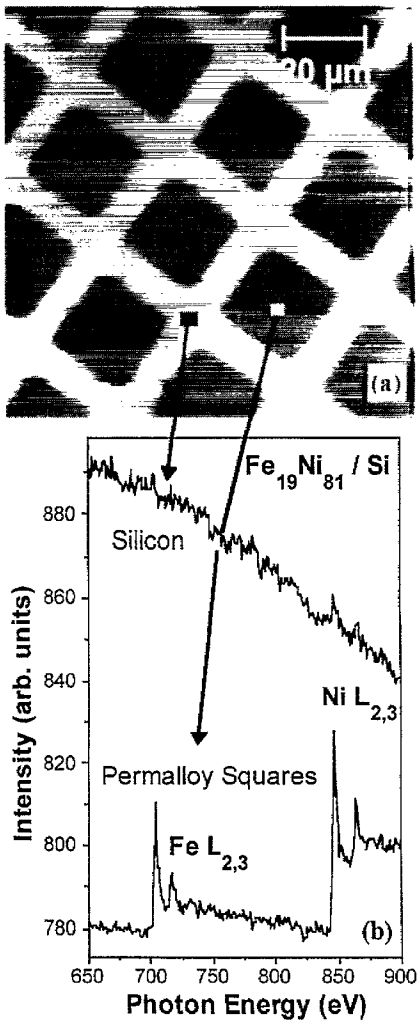

Fig. 4. Photoemission microscopy and microspectroscopy from a permalloy pattern on Si. Top panel: Pattern imaged at the Fe L_3 edge. Bottom panel: X-ray absorption spectra from two selected areas marked in the image.

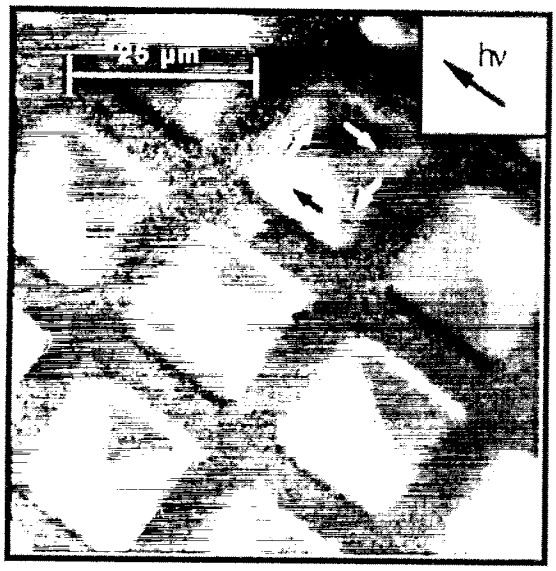

Fig. 5. Magnetic domain pattern in the permalloy pattern shown in Fig. 4. Magnetic contrast is due to magnetic circular dichroism at the Fe $L_{2,3}$ edges. The arrow indicates the direction of incidence of the circularly polarized light.

which is indicated by the arrows. The magnetization in the two domains with the same intermediate gray level is normal to the photon wave vector $\boldsymbol{q}$.

The domain pattern in the square is a simple flux closure structure. It is mainly determined by the shape of the permalloy patches. The reason for this domain pattern is the very small magnetocrystalline anisotropy of permalloy. As a consequence, the behavior of the magnetization in the present case is dominated by the tendency of the system to minimize the magnetic stray field. This results in the characteristic arrangement of four triangular domains observed in the experiment. This ideal case is easily affected by defects, as can be seen in the square in the center of the image. It shows a more complex pattern, presumably pinned by a structural defect on the substrate. In passing, we note that the same information about the magnetic microstructure is obtained at the Ni $L_{2,3}$ edges. The selected area absorption spectroscopy used to obtain the spectra in Fig. 2 can also be employed to record local magnetic circular dichroism spectra from micron-sized regions [40].

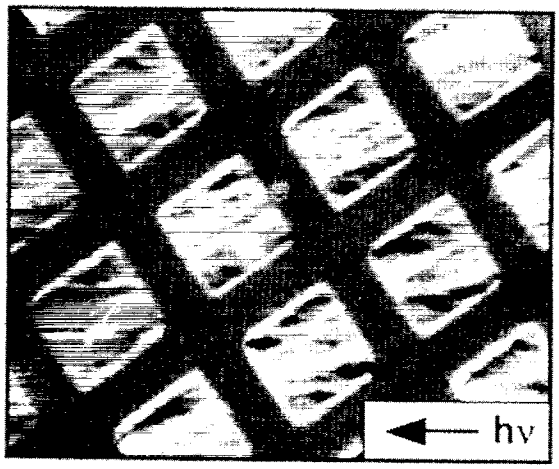

Fig. 6. Magnetic domain pattern in a patterned CoPt multilayer grown on Si. Image recorded at the Co L_3 edge. Side length of a square is 20 µm.

A completely different situation is encountered in the second microstructured sample. This was a Co Pt multilayer (7 periods of 21 Å Pt and 25 Å Co) grown on a Si substrate. The top Pt layer also served as a protective coating. After growing the multilayer by DC sputtering techniques the sample was covered with a photoresist and illuminated with UV-light through a mesh. After dissolving the photoresist from the unexposed areas the sample was patterned by reactive ion etching, resulting in well-defined squares of ca. 20 µm side length. In a last step the residual photoresist was removed before introducing the sample into the UHV system. The magnetic domain pattern (Fig. 6) is extracted by subtracting two images recorded at the Co L_3 edge with opposite helicity. The filigran featherlike domain pattern in each square reflects the strong influence of the intrinsic anisotropy in the CoPt system. A statistical analysis of the abundance of the various gray levels in the CoPt squares exhibits an almost continuous distribution, whereas we found only three distinct maxima for the permalloy squares in Fig. 5. This suggests that the magnetization vector in the CoPt system is more randomly oriented which is compatible with the multilayer being polycrystalline. In this case the easy axes of magnetization – as determined by the

magnetocrystalline anisotropy – change with the spatial orientation of the individual crystallite. The strong ferromagnetic coupling of neighboring grains, however, permits only a small deviation of the local magnetization vector from the average macroscopic direction of the magnetization $\boldsymbol{M}$. The result is a rather complex variation of $\boldsymbol{M}$ along the sample surface which is sometimes called a magnetization 'ripple'.

It must be pointed out that the image in Fig. 6 shows only a partial view of the domain pattern, because only the component of $\boldsymbol{M}$ along the incident light beam is mapped. For a simple domain structure such as in Fig. 5 this is sufficient to reconstruct the complete pattern by flux closure arguments. In more complicated structures (Fig. 6) an in situ rotation of the sample with respect to the incoming photon beam is required in order to obtain a complete picture. Such a device will be added to the instrument in the near future.

5. Sensitivity and depth of information

5.1. Depth of information

The magnetic contrast in photoemission microscopy is generated by magnetic circular dichroism in the total electron yield. The major contribution to the image is supplied by low-energy secondary electrons. Another domain imaging method which draws its magnetic information from secondary electrons – more precisely from their spin polarization – is SEMPA. Despite the fact that both methods PEEM and SEMPA use the same electrons for the image formation, the depth of information significantly differs in these two cases. The spin polarization of the secondary electrons is a result of the spin-dependence of the inelastic scattering cascade in a ferromagnetic material and reflects the orientation of $\boldsymbol{M}$ in the region where these secondary electrons have been created. Minority spin electrons have a higher scattering probability because the spin-down unoccupied density of states at the Fermi level is higher. The emitted secondary electrons are therefore highly spin-polarized with a majority spin character [17]. This scattering process acts as an internal 'spin filter' and is very effective at low kinetic energies. As a consequence, the high-spin polarization of the secondary electrons is connected to a small depth of information (typically 5 Å [6, 41]).

The situation in photoemission microscopy is significantly different. The magnetic information in a PEEM is already introduced within the primary excitation step. The magnetic dichroism in the photoabsorption translates into a difference in the Auger electron creation for regions with a local magnetization vector parallel or antiparallel to the incoming photon beam. On their way to the surface these highly energetic Auger electrons generate a cascade of inelastically scattered secondary electrons which again contain the magneto-dichroic signal. In a simple picture the depth of information will therefore be determined by the stopping power of the Auger electrons rather than by their inelastic mean free path (typically 15–20 Å for LMV Auger transitions from 3d transition metals [42]) or the inelastic mean free path of the low-energy secondary electrons. In a more detailed approach one will have to consider a complicated convolution of the stopping power of the high-energy Auger electrons and the mean free path length of the low-energy secondary electrons which also has to take into account the specific experimental goemetry (angle of acceptance). In any case, the information depth in magnetic domain imaging using a PEEM is significantly larger than that in a SEMPA experiment. Together with the chemical selectivity of the excitation process this property can be conveniently exploited to investigate buried surfaces and layers, and image magnetic microstructures in systems covered by non-magnetic overlayers [14].

The large information depth in PEEM can be used to separate the individual contributions in a magnetically coupled overlayer system. This is shown in Fig. 7. We have grown a Cr wedge with a thickness ranging from 0–10 ML on an Fe(0 0 1) whisker and covered it by a Co cap layer (5 ML). Both the Cr and the Co layer were deposited at 200°C. Subsequently, we recorded a set of images below and at the Cr, Fe, and Co L_3 edges for the same light helicity. The particularly simple domain pattern in the Fe whisker, namely, two oppositely magnetized domains, is clearly visible already in the raw image. The magnetic contrast disappears if the

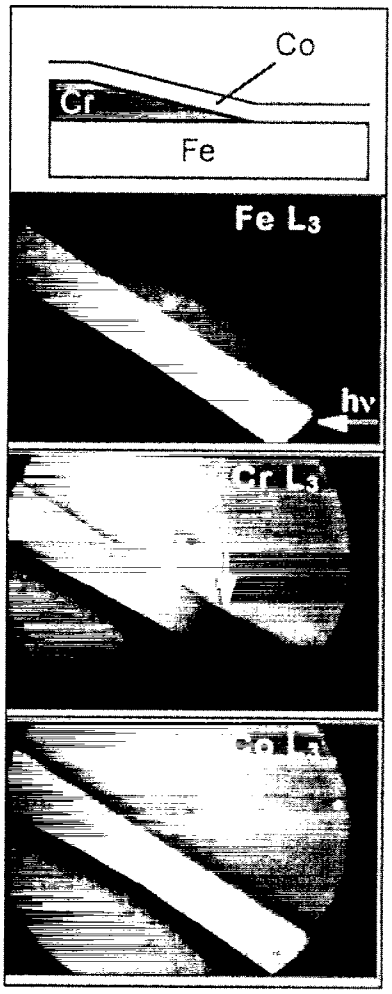

Fig. 7. Magnetic domain patterns in a Co/Cr-wedge/Fe(1 0 0) sandwich acquired in the survey mode. The images at the Fe (upper), Cr (central), and Co L_3 edges (bottom) have been recorded from the completed sandwich. The Cr wedge ranges from 0–10 ML (onset marked by the arrow, highest coverage in the upper left-corner), the Co overlayer has a thickness of 5 ML. The width of the Fe whisker is about 140 μm.

excitation energy is set below the absorption edge. The subtraction of the two images enhances the chemical selectivity. Remember that this image shows the magnetic domain pattern of Fe through the Cr and Co overlayers. In the Cr images we see the onset of the wedge (marked by arrow) and an increase of the Cr signal along the whisker axis towards the upper left corner of the image. No magnetic signal can be resolved in the Cr layer. The increase of the Cr thickness is also reflected in a small reduction of the Fe signal. At the Co edge we again see a clear magnetic structure in the image. This domain pattern is identical to that observed in Fe and does not change with the Cr layer thickness. The Co top layer is obviously ferromagnetically coupled to the Fe(0 0 1) substrate in the investigated Cr thickness regime up to 10 ML.

The results show that in this particular system the magnetic domains in the Fe substrate remain clearly visible through a 15 ML (ca. 25 Å) thick metallic overlayer even in a single image. In this case no use has been made of a magnetic contrast enhancement by reversing the light helicity. If a difference of images taken at opposite helicities is considered we estimate that a reasonable magnetic signal may be obtained even from a surface buried as deep as 25–30 ML.

5.2. Sensitivity

It may be inferred from the above results that the relatively large depth of information leaves the method not sensitive enough to detect a magnetic signal in small quantities of a given material. In order to evaluate the limitations of the technique in this respect, we investigated the magnetic signal from Cr films in the sub-monolayer regime. The Cr films were grown as discontinuous wedges consisting of a sequence of equidistant terraces of 10 μm width ('staircase'). Each terrace corresponds to an increment of the Cr coverage by 0.1 ML. The films were grown at elevated temperature (200°C), in order to make connections with previous results [27]. As is accepted by now, these growth conditions favor the formation of a CrFe interfacial alloy [43]. This leads to a magnetic frustration and a presumably reduced magnetic moment of Cr [44, 45], thereby reducing the MCD signal. It may therefore be considered a critical test case.

The images taken at the Cr L_3-edge show a regular pattern in the intensity distribution (Fig. 8). Starting from the lowest coverage of 0.1 ML, the intensity of the Cr signal increases linearly with each incremental step in the coverage. The individual images do not directly exhibit a magnetic

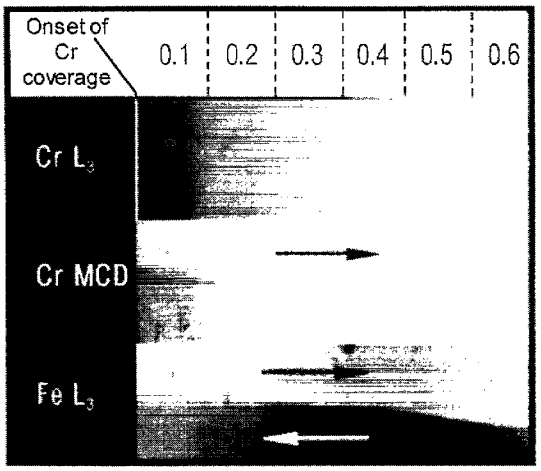

Fig. 8. Chemical (top) and magnetic contrast (center) in a stepped Cr layer on Fe(0 0 1). Asymmetry image recorded at the Cr L_3 edge (top, center) and difference image at the Fe L_3 edge (bottom). The Cr coverage increases from the left to the right in units of 0.1 ML.

contrast. The asymmetry calculation (Eq. (3)) from two images taken at opposite helicities reveals a small but distinct magnetic signal. The domain structure in the Cr film is determined by the coupling to the Fe substrate. The maximum magnetic contrast in the Cr image amounts to only about $A \approx 0.8\%$ intensity asymmetry. Despite this fact, we are able to discern the magnetic contrast already at the smallest film thickness of 0.1 ML. The acquisition time for each of the two raw images used to calculate the Cr asymmetry picture was about 10 min.

Comparing the magnetic structure of the Cr film in the submonolayer regime to that in the Fe substrate, we note that the contrast in the Cr image is not reversed as should be expected for an antiferromagnetic coupling between Fe and Cr. This finding is in contrast to previous results for a full Cr monolayer for which an antiferromagnetic coupling was found under the nominally same preparation conditions [27]. The reasons for this discrepancy, for example, a different surface morphology, are not yet clear and further investigations are necessary to clarify this change in the coupling character in the submonolayer regime.

6. Mesoscopic magnetic structures: domain walls

6.1. Domain wall contrast

The last example outlines the high chemical and magnetic sensitivity of the technique and demonstrates that magnetic information even on the submonolayer scale may be obtained with reasonable acquisition times.

The transition region between two neighboring domains, the so-called domain wall, represents a magnetic structure on a yet smaller lateral (mesoscopic) scale. The task of mapping these domain walls is thus another crucial test for the capabilities of a magnetic domain imaging technique. The directional characteristics of MCD can be exploited to selectively image the magnetization component within a domain wall along the direction of light incidence. An example is given in Fig. 9 which shows a small section from an Fe(1 0 0) single-crystal surface. The crystalline symmetry of this surface is fourfold. In BCC-Fe, the easy axes of magnetization are the [1 0 0] directions. As a consequence, there are four easy directions for $\boldsymbol{M}$ in the (1 0 0) surface. In Fig. 9 we have chosen a region of the sample where $\boldsymbol{q} \perp \boldsymbol{M}$ holds for most of the area which therefore shows up in a medium gray level. No areal domain contrast can be discerned in this

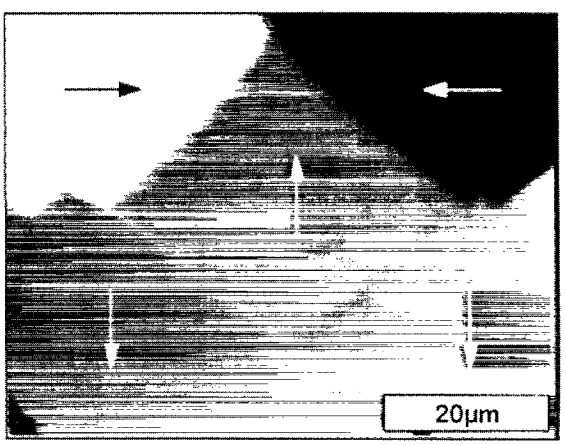

Fig. 9. Magnetic domain pattern on a Fe(0 0 1) surface. Arrows mark the local orientation of the magnetization. Light incidence along the horizontal axis.

region. Exceptions are the domains in the upper left- and right-corner of the image. Their dark and bright contrasts indicate a parallel and antiparallel alignment of M and q. Starting from these domains a bright and a dark narrow line meet below the center of the image. They bound a diamond-shaped region. These lines originate from domain walls and suggest that there is an additional domain structure in this region. Particularly, the magnetization in the diamond must be oriented opposite to M in the adjacent areas with the same gray level. Based on this information, we can reconstruct the domain pattern even in the region with $q \perp M$.

In order to understand the domain-wall contrast observed in the experiment we must consider the difference between domain walls in the bulk and at the surface. For this purpose we will assume first a simple 180° wall in the bulk. Across this wall, the magnetization vector rotates continuously by 180° from one orientation to the other. The axis of rotation stands normal to the wall. This case is called a Bloch wall. Note that for in-plane magnetization the magnetization vector in the center of the Bloch wall stands normal to the surface plane. Translating this Bloch-like rotation of M to the surface would generate a significant magnetization component normal to the surface. An energetically more favorable situation is achieved, if the magnetization vector rotates within the surface, i.e., the rotational axis lies within the wall plane and normal to the surface. This behavior is said to be Néel-like. Consequently, the Bloch wall in the bulk takes a Néel-like termination at the surface.

The situation in the present case is more complicated because the domain configuration at the surface is stabilized by the underlying bulk. This can be seen simply from the fact that the arrangement of M in Fig. 9 is energetically unfavorable and would be forbidden by stray field arguments if only the surface was concerned. The diamond resembles a classical Lifshitz flux closure structure which is formed when the magnetization in the bulk is oriented perpendicular to the surface [46]. The dark and bright lines in Fig. 9 should thus be interpreted as the so-called V-lines [47]. These are the result of two 90° walls in the bulk meeting at the surface.

6.2. Limitations of the lateral resolution

The width of these V-lines in our experiment has been determined to $d \approx 500$ nm. The best 'magnetic' resolution that we have obtained so far was $d \approx 300$ nm and has been measured across a simple 180° domain wall in Fe(0 0 1). This value must be compared to the width of the domain wall in the same system of around 200 nm, as measured by SEMPA [48]. Obviously, the resolution in magnetic PEEM is still lower than the actual domain wall width. Since the instrumental resolution is far better than 300 nm, the reason must lie in the process of image formation itself. The limiting factor for the resolution – not only of magnetic microstructures – is the energy spread of the secondary electrons which build up the image. Through the chromatic aberration of the objective lens this energy spread causes a broadening of the features in the image. In order to push the lateral resolution to the instrumental limits the energy spread must be reduced. This implies the use of an imaging energy filter which will be implemented into the next generation of the instrument.

7. On the feasibility of laboratory experiments

The experimental approaches described in the previous section rely on the use of tunable circularly polarized synchrotron radiation. The worldwide ongoing development and construction of third generation storage ring facilities improves the availability of highly brilliant sources of this type of light, in particular, in the soft X-ray regime. Nevertheless, one would also like to have the possibility of carrying out some experiments without resorting to a storage ring. Therefore, some efforts have been devoted to the search for alternative approaches. In solving this task it is of help that magnetic linear dichroism in photoemission (MLDAD) can be observed even with unpolarized light [49–51]. In this case the magneto-dichroic signal amounts to about half the value observed with linearly polarized light. In other words, conventional X-ray tubes can be employed for the photoexcitation without the need of additional polarization optics. In

order to obtain magnetic sensitivity and elemental selectivity, a proper energy filtering of the image is required, of course. In addition, recalling the discussion in Section 2.2, a sufficient angular resolution is necessary as well. This leaves an imaging electron spectrometer as the instrument suited best for the purpose of performing a feasibility study.

The results compiled in Fig. 10 show that the mapping of magnetic domains using the approach discussed above is indeed feasible [34]. The data have been obtained with a VG ESCASCOPE, irradiating the sample with a 300 W X-ray tube with a Mg Kα anode. The sample was an iron single crystal with (0 0 1) surface orientation. The upper panel shows the MLDAD spectrum at the Fe 2p photoemission lines observed with the unpolarized radiation, and recorded in the spectrum mode of the instrument by reversing the magnetization of the iron sample. This result is fully consistent with the previous findings from experiments employing the excitation with linearly polarized light [52]. The distinct dichroism at the Fe $2p_{3/2}$ line was then employed for imaging purposes in the following way. First, an image was acquired with the kinetic energy of the electrons set to the maximum of the positive excursion of the MLDAD signal at the $2p_{3/2}$ line. Then a second image was recorded at the energy position of the maximum negative excursion of the asymmetry at the same line. Since the magnetic signal at this energy is significantly smaller, this second image was merely used to normalize the first one. This sequence was repeated a number of times and the individual images were added up in order to reduce the statistical scatter in the calculated asymmetry image. The final result of this experiment is displayed in the bottom panel of Fig. 10 and shows a region of the crystal surface with two oppositely magnetized domains, i.e., a simple 180° domain wall. The contrast between the two domains is clearly visible. An accumulated line scan perpendicular to the domain wall reveals a maximum contrast level of the order of 2%. It should be pointed out that a total of about 6 h of data acquisition time was needed to bring the statistical scatter to the level shown. A significant reduction of the acquisition time may be achieved by focusing the light of the X-ray tube down to the field of view of the instrument (800 μm) by means of a suitable X-ray optical device. The lateral resolution which can be reached with this type of imaging electron spectrometer is limited to several μm, and thus cannot compete with a PEEM. It remains to be seen whether or not a magneto-dichroic contrast mechanism with unpolarized light can be employed in a cathode lens microscope with imaging energy filter, too. First, experiments showing MDAD in threshold photoemission yielded promising results [53].

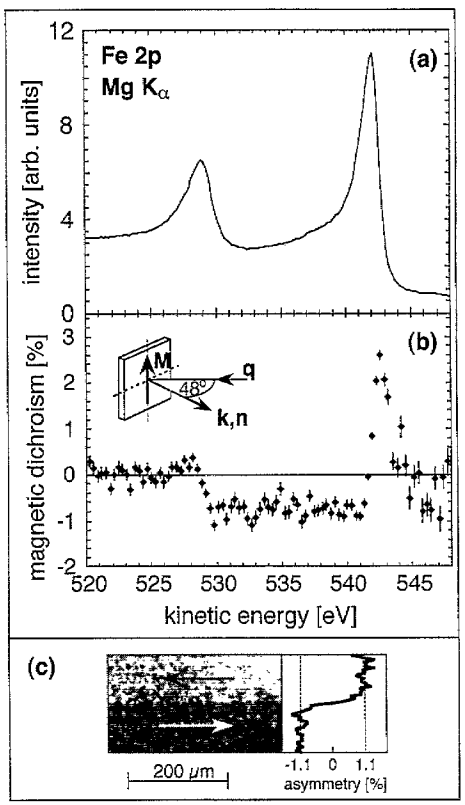

Fig. 10. Magnetic studies on an Fe(1 0 0) surface employing linear magnetic dichroism (MLDAD) with unpolarized X-rays. (a) Photoemission spectrum of the Fe 2p core levels, (b) corresponding magnetic dichroism (MLDAD) spectrum obtained upon magnetization reversal, (c) magnetic domains observed by means of an imaging electron spectrometer using the MLDAD signal at the Fe $2p_{3/2}$ photoemission line as a contrast mechanism.

8. Conclusions and outlook

In this contribution the current status and limitations of photoemission microscopy using X-ray magnetic dichroism have been outlined. This technique should be seen as a complement rather than a competition to established domain-imaging methods. Its most important virtue is a unique combination of magnetic sensitivity and chemical selectivity, paired with a parallel and thus fast data acquisition. The technique is already capable of imaging single-domain walls and resolve very small magnetic signals from submonolayer coverages of magnetic materials. A further improvement of the lateral resolution requires the implementation of an imaging energy filter. An interesting future issue will be the possibility of time-resolved studies. The domain contrast in, for instance, Fe and Ni single crystals is large enough to be imaged by a conventional video system. This will allow one to follow the changes in the magnetic microstructure at least with TV rates.

Acknowledgements

Financial support by the Bundesminister für Bildung und Forschung through Grant No. 05 644 EFA is gratefully acknowledged. The author wants to express his gratitude to R. Frömter, M. Seider, Ch. Ziethen, O. Schmidt, W. Swiech, G. Schönhense, M. Neuber, M. Grunze and J. Kirschner for very fruitful collaborations. Thanks go to A. Wadas and R. Wiesendanger (University of Hamburg) for making the permalloy microstructure available. The CoPt multilayer microstructure was generously supplied by P. Schicketanz and M. Huth from the University of Mainz. The help of F. Schäfers (BESSY) and N.B. Brookes (ESRF) during the beamtimes proved to be invaluable.

References

[1] J. Kranz, A. Hubert, Z. Angew. Phys. 15 (1963) 220.
[2] F. Schmidt, W. Rave, A. Hubert, IEEE Trans. Magn. 21 (1985) 1596.
[3] E. Fuchs, Naturwiss. 47 (1960) 392.
[4] J.N. Chapman, J. Phys. D 17 (1984) 623.
[5] K. Koike, K. Hayakawa, Jpn. J. Appl. Phys. 23 (1984) L187.
[6] H.P. Oepen, J. Kirschner, Scann. Microsc. 5 (1991) 1.
[7] M.R. Scheinfein, J. Unguris, M.H. Kelley, D.T. Pierce, R.J. Celotta, Rev. Sci. Instr. 61 (1990) 2501.
[8] Y. Martin, H.K. Wickramasinghe, Phys. Rev. Lett. 50 (1987) 1455.
[9] A. Wadas, P. Rice, J. Moreland, Appl. Phys. A 59 (1994) 63.
[10] M. Hehn, K. Ounadjela, J.P. Bucher, F. Rousseaux, D. Decanini, B. Bartenlian, C. Chappert, Science 272 (1996) 1782.
[11] M.W.J. Prins, R.H.M. Groeneveld, D.L. Abraham, H. van Kempen, H.W. van Kesteren, Appl. Phys. Lett. 66 (1995) 1141.
[12] P. Fischer, T. Eimüller, G. Schütz, G. Schmahl, P. Guttmann, D. Raasch, Z. Phys. B 101 (1996) 313.
[13] M.S. Altman, H. Pinkvos, J. Hurst, H. Poppa, G. Marx, E. Bauer, Mat. Res. Soc. Symp. Proc. 232 (1991) 125.
[14] J. Stöhr, Y. Wu, M.G. Samant, B.D. Hermsmeier, G. Harp, S. Koranda, D. Dunham, B.P. Tonner, Science 259 (1993) 658.
[15] C.M. Schneider, K. Holldack, M. Kinzler, M. Grunze, H.P. Oepen, F. Schäfers, H. Petersen, K. Meinel, J. Kirschner, Appl. Phys. Lett. 63 (1993) 2432.
[16] C.M. Schneider, Z. Celinski, M. Neuber, C. Wilde, M. Grunze, K. Meinel, J. Kirschner, J. Phys.: Condens. Matter 6 (1994) 1177.
[17] G. Chrobok, M. Hofmann, G. Regenfus, R. Sizmann, Phys. Rev. B 15 (1977) 429.
[18] J. Kirschner, in: R. Feder (Ed.), Polarized Electrons in Surface Physics, World Scientific, Singapore, 1985.
[19] D. Tillmann, R. Thiel, E. Kisker, Z. Phys. B 77 (1989) 1.
[20] G.V. Spivak, T.N. Dombrovskaia, N.N. Sedov, Sov. Phys. Dokl. 2 (1957) 120.
[21] M. Mundschau, J. Romanowicz, J.Y. Wang, D.L. Sun, H.C. Chen, J. Vac. Sci. Technol. B 14 (1996) 3126.
[22] G. Schütz, W. Wagner, W. Wilhelm, P. Kienle, R. Zeller, R. Frahm, G. Materlik, Phys. Rev. Lett. 58 (1987) 737.
[23] L. Baumgarten, C.M. Schneider, F. Schäfers, H. Petersen, J. Kirschner, Phys. Rev. Lett. 65 (1990) 492.
[24] C. Roth, F.U. Hillebrecht, H.B. Rose, E. Kisker, Phys. Rev. Lett. 70 (1993) 3479.
[25] U. Fano, Phys. Rev. 178 (1969) 131.
[26] C.T. Chen, F. Sette, Y. Ma, S. Modesti, Phys. Rev. B 42 (1990) 7262.
[27] C.M. Schneider, K. Meinel, J. Kirschner, M. Neuber, C. Wilde, M. Grunze, K. Holldack, Z. Celinski, F. Baudelet, J. Magn. Magn. Mater. 162 (1996) 7.
[28] B.P. Tonner, G.R. Harp, S.F. Koranda, J. Zhang, Rev. Sci. Instr. 63 (1992) 564.
[29] F.U. Hillebrecht, T. Kinoshita, D. Spanke, J. Dresselhaus, C. Roth, H.B. Rose, E. Kisker, Phys. Rev. Lett. 75 (1995) 2224.
[30] D. Venus, Phys. Rev. B 43 (1993) 6144.
[31] G. van der Laan, Phys. Rev. B 51 (1995) 240.
[32] F.U. Hillebrecht, H.B. Rose, T. Kinoshita, Y.U. Idzerda, G. van der Laan, R. Denecke, R. Ley, Phys. Rev. Lett. 75 (1995) 2883.

[33] B.P. Tonner, D. Dunham, T. Droubay, M. Pauli, J. Electron Spectr. Rel. Phen. 1996, in press.
[34] P. Coxon, J. Krizek, M. Humpherson, I.R.M. Wardell, J. Electron Spectr. Rel. Phen. 51/52 (1990) 821.
[35] H. Petersen, C. Jung, C. Hellwig, W.B. Peatman, W. Gudat, Rev. Sci. Instr. 66 (1995) 1.
[36] P. Elleaume, J. Synchrotron Rad. 1 (1994) 19.
[37] C.T. Chen, Rev. Sci. Instr. 63 (1992) 1229.
[38] M. Drescher, G. Snell, U. Kleineberg, H.-J. Stock, N. Müller, U. Heinzmann, N.B. Brookes, Rev. Sci. Instr. 68 (1997) 1939.
[39] E. Bauer, W. Telieps, in: A. Howie, U. Valdrè (Eds.), Surface and Interface Characterization by Electron Optical Methods, Plenum Press, New York, 1988, p. 195.
[40] W. Swiech, G.H. Fecher, C. Ziethen, O. Schmidt, G. Schönhense, K. Grzelakowski, C.M. Schneider, R. Frömter, J. Kirschner, J. Electron Spectr. Rel. Phen. 84 (1996) 171.
[41] D.L. Abraham, H. Hopster, Phys. Rev. Lett. 58 (1987) 1352.
[42] M.P. Seah, W.A. Dench, Surf. Interf. Anal. 1 (1979) 1.
[43] D. Venus, B. Heinrich, Phys. Rev. B 53 (1996) R1733.
[44] D. Stoeffler, F. Gauthier, J. Magn. Magn. Mater. 147 (1995) 260.
[45] D. Stoeffler, F. Gauthier, Phys. Rev. B 44 (1991) 10389.
[46] S. Chikazumi, Physics of Magnetism, Wiley, Krieger, New York, 1964.
[47] R.W. DeBlois, J.C.D. Graham, J. Appl. Phys. 29 (1958) 931.
[48] H.P. Oepen, J. Kirschner, Phys. Rev. Lett. 62 (1989) 819.
[49] M. Getzlaff, C. Ostertag, G.H. Fecher, N.A. Cherepkov, G. Schönhense, Phys. Rev. Lett. 73 (1994) 3030.
[50] F.U. Hillebrecht, W.-D. Herberg, Z. Phys. B 93 (1994) 299.
[51] C.M. Schneider, W. Kuch, U. Pracht, A. Chassé, J. Kirschner, Phys. Rev. B 54 (1996) R15618.
[52] F.U. Hillebrecht, C. Roth, H.B. Rose, W.G. Park, E. Kisker, N.A. Cherepkov, Phys. Rev. B 53 (1996) 12182.
[53] G.K.L. Marx, M.D. v. Przychowski, G. Schönhense, J. Henk, R. Feder, C.M. Schneider, Phys. Rev. Lett. 1997, submitted.